BUILDING RECONSTRUCTION BASED ON A SMALL NUMBER OF TRACKS USING NONPARAMETRIC SAR TOMOGRAPHIC METHODS

M. Omati [1], M. M. Omati [2] *, M. H. Bastani [3]

[1] Faculty of Geodesy and Geomatics Engineering, K. N. Toosi University of Technology, Tehran, Iran – m.omati@yahoo.com
[2] Faculty of Electrical Engineering, Sharif University of Technology, Tehran, Iran – Mohammad_omati@yahoo.com
[3] Faculty of Electrical Engineering, Sharif University of Technology, Tehran, Iran – bastanih@sharif.edu

Commission IV, WG IV/3

KEY WORDS: Building Reconstruction, Tomographic Synthetic Aperture Radar (TomoSAR), Nonparametric Spectral Analysis techniques, Maximum Entropy method, Linear Prediction Estimator, Minimum Norm algorithm.

ABSTRACT:

Nowadays, the synthetic aperture radar (SAR) tomography (TomoSAR) technique plays a notable role in the 3D reconstruction of urban buildings through several SAR acquisitions with slightly different positions. Nonparametric-based TomoSAR spectral estimation algorithms usually work well when a large number of SAR observations. In this study, with a limited number of SAR images, we have assessed the efficiency of the nonparametric spectral estimation methods, including maximum entropy (ME), singular value decomposition (SVD), linear prediction (LP), Capon, minimum norm (MN), and beamforming (BF) in the reconstruction of the third dimension of urban buildings. The experiments are conducted on both simulated and TerraSAR-X stripmap images to indicate the effectiveness of the LP proposed estimation algorithm. The analysis of the results proves that by minimizing the average output signal power over the antenna array elements, the LP spectral estimation achieves the discrimination of distinct scatterers inside an image pixel. In addition, this low computational estimator improves the sidelobe suppression and the height estimates of the scatterers in the complex multiple-scattering urban environment. Compared to SVD, maximum entropy, Capon, minimum norm, and beamforming, the height of the Eskan tower in Tehran, Iran, obtained with the LP technique, is considerably near to field-based measurement.

1. INTRODUCTION

Synthetic aperture radar (SAR) employs the coherent nature of the radiation to earn considerable discrimination capabilities in the azimuth and range direction (Franceschetti and Lanari, 1999). High resolution in the range is typically acquired by focusing on a transmitted long-duration (large bandwidth) linear frequency modulated pulse. In contrast, high resolution in the azimuth direction is attained by synthesizing a large azimuth aperture starting from the data amassed along the acquisition track by a limited-size real antenna that coherently radiates the scene at regular intervals.

SAR forms 2D images of the terrain in both the range and azimuth direction. But, the obtained image is only a projection of the area, which yields several problems. One case is that it is impossible to access the third dimension using a single image. Another problem is the difference between the values of each point and the authentic values (Baselice et al. 2009).

The synthetic aperture radar interferometry (InSAR) approach, which relies on the signal phase differences between two image passes (Bamler and Hartl, 1998), expresses a valuable case of multiple acquisitions and can build a three-dimensional (3D) terrain surface construction. Nonetheless, the InSAR method considers that scatterers only have been spread on the surface of the expected object. Also, InSAR needs nonlinear processing, specifically when dealing with layover and foreshortening areas, to the phase unwrapping of the calculable wrapped phase distinctions. SAR tomography (TomoSAR), tempting significant attention in urban scenarios, has been proposed to surmount this constraint (Omati et al. 2021).

Parallel and circular are two primary classes of tomography. In parallel tomography, the dispatched beams are nearly parallel, meaning the dissimilarity in the acquisition angles is extremely slight. TomoSAR is known as a class of parallel tomography. Nevertheless, circular tomography acquires images from various angles around the target. In the projection-slice theorem, if the number of projections of the desired object at an infinite number of angles is limitless, the reconstruction of the 3D model of the original object is possible. Because of the difference in the range direction for each pixel, the height cannot be assessed using a linear function. To find the non-linear function, some parameters, such as the precise acquisition angle, the swath width, and the resolution in each direction, is essential. TomoSAR, as an evolved form of InSAR, is a multi-track approach that utilizes several SAR images from the same region to discover the number of scatterers and assess the reflectivity profile along the elevation direction for each image pixel.

With the release of high-resolution space-based SAR satellites, such as TanDEM-X and TerraSAR-X, the efficient use of very high-resolution SAR images has attracted the attention of many researchers in urban mapping. Many scholars have also proposed many algorithms for TomoSAR imaging, such as Fourier transform methods and spectral estimation methods

* Corresponding author

https://doi.org/10.5194/isprs-annals-X-4-W1-2022-617-2023

(Reigber and Moreira, 2000) and (Fornaro et al. 2003). However, due to the limitation of the acquisitions and the irregular baselines of the spaceborne SAR system, the 3D reflectivity profile reconstructed by the algorithms above is usually inefficient.

Standard spectral estimation algorithms are divided into three categories: compressive sensing (CS) (Zhu and Bamler, 2010), parametric, and nonparametric methods (Wei et al. 2014). The nonparametric benefit over the other two techniques is that it usually produces a dense spectrum whose positions of peaks are clarified as locations of scatterers in the direction of elevation (Gini et al. 2002). Also, the number and the indefinite parameters of scatterers are directly assessed using the SAR images (Wei et al. 2014). Well-known nonparametric Direction-of-Arrival (DOA) estimation approaches such as the Capon method, Beamforming, and so forth can be executable. Nevertheless, due to the small number of observations, tomographic inversion in nonparametric spectral estimators is often challenging.

This paper attempts to assess the capability of nonparametric spectral estimation algorithms in a case study with complex geometry, based on a small number of SAR tracks. Considering that, three nonparametric spectral estimators in TomoSAR application, i.e., minimum norm (MN), linear prediction (LP), and maximum entropy (MP) in the placement position of the three buildings with equal height adjacent to each other, are evaluated. This study aims to improve the TomoSAR reconstruction quality and the building height estimation for the limited amount of images. In this used complex case study, the obtained results indicate the capability of the proposed LP spectral estimation algorithm to distinguish different scatterers in an image pixel, reduce the sidelobe effect, and the low difference between the estimated height and the ground-truth value.

2. METHODOLOGY

2.1 Basic TomoSAR Theory

As a multi-baseline extension of conventional cross-track SAR interferometry, TomoSAR provides complete 3D imaging by organizing a synthetic aperture principle along the perpendicular direction to both slant range and azimuth directions. This arrangement can be consecutive, with a single SAR sensor acquiring data at different times.

If the SAR sensor observes the same area by N times, the received signal g_n from all of the scatterers of the n^{th} image for the pixel (x,r) of the azimuth range cell is formulated as follows:

$$g_n(x,r) = \int \gamma(s) exp(-j\,2\pi\xi_n s)ds + \varepsilon_n(x,r) \tag{1}$$

where $\gamma(s)$ = complex received reflectivity of the scatterer

$\xi_n = \dfrac{2b_{\perp n}}{\lambda r}$ = spatial frequency along the elevation

r = distance between pixel and the reference antenna

λ = wavelength parameter

$b_{\perp n}$ = vertical component of the spatial baseline

$\varepsilon_n(x,r)$ = noise term

Due to the existence of the limited number of scatterers in each pixel, we can discretize s to the L backscattered positions uniformly with a step equal to Δs :

$$g_n(x,r) = \sum_{s=s_1}^{s_L} \gamma(s) exp(-j\,2\pi\xi_n s)ds + \varepsilon_n(x,r) \tag{2}$$

The equation (2), in the form of a matrix, changes to:

$$\underbrace{\begin{bmatrix} g_1(x,r) \\ g_2(x,r) \\ g_3(x,r) \\ \vdots \\ g_N(x,r) \end{bmatrix}}_{\mathbf{g}} = \underbrace{\begin{bmatrix} \overbrace{e^{j2\pi\xi_1 s_1}}^{\mathbf{a}(s_1)} & \overbrace{e^{j2\pi\xi_1 s_2}}^{\mathbf{a}(s_2)} & \cdots & \overbrace{e^{j2\pi\xi_1 s_L}}^{\mathbf{a}(s_L)} \\ e^{j2\pi\xi_2 s_1} & e^{j2\pi\xi_2 s_2} & \cdots & e^{j2\pi\xi_2 s_L} \\ e^{j2\pi\xi_3 s_1} & e^{j2\pi\xi_3 s_2} & \cdots & e^{j2\pi\xi_3 s_L} \\ \vdots & \vdots & \ddots & \vdots \\ e^{j2\pi\xi_N s_1} & e^{j2\pi\xi_N s_2} & \cdots & e^{j2\pi\xi_N s_L} \end{bmatrix}}_{\mathbf{A}} \underbrace{\begin{bmatrix} \gamma(s_1) \\ \gamma(s_2) \\ \gamma(s_3) \\ \vdots \\ \gamma(s_L) \end{bmatrix}}_{\boldsymbol{\gamma}} + \underbrace{\begin{bmatrix} \varepsilon_1(x,r) \\ \varepsilon_2(x,r) \\ \varepsilon_3(x,r) \\ \vdots \\ \varepsilon_N(x,r) \end{bmatrix}}_{\boldsymbol{\varepsilon}} \tag{3}$$

$$\mathbf{g} = \mathbf{A}\boldsymbol{\gamma} + \boldsymbol{\varepsilon}$$

where $\mathbf{A} = [\mathbf{a}(s_1) \;\; \mathbf{a}(s_2) \;\; \cdots \;\; \mathbf{a}(s_L)]$ = $N \times L$ matrix related to the SAR acquisition geometry

$\mathbf{a}(s_i)$ = its i^{th} column vector

To estimate the 3D reflectivity function $\boldsymbol{\gamma}$, first, a stack of collected range-azimuth images is pre-processed to remove the flat-earth phase component and the phase errors introduced by atmospheric propagation. Then, DOA-based estimation methods can be applied to the processed SAR images. In the following, we inset three nonparametric spectral estimation methods with TomoSAR application for the robust height reconstruction of buildings.

2.2 Spectral Estimation methods in TomoSAR

2.2.1 Linear Prediction Estimation Algorithm: The DOA estimation technique based on spectral LP is widely applied in fields like time series, spectrum estimation, and array signal processing models (Makhoul, 1975). The proposed LP approach is based on minimizing the output average power of signal over the antenna array (Gamba, 2020). Thus, in the stack of SAR images, the proposed method is considered robust in improving building height retrieval and TomoSAR reconstruction.

2.2.2 Linear Prediction Estimation Algorithm: The DOA estimation technique based on spectral LP is widely applied in fields like time series, spectrum estimation, and array signal processing models (Makhoul, 1975). The proposed LP approach is based on minimizing the output average power of signal over the antenna array (Gamba, 2020). Thus, in the stack of SAR images, the proposed method is considered robust in improving building height retrieval and TomoSAR reconstruction.

The predictive coefficients, $\gamma(s_l)$, in a weighted linear combination of $\exp[-j2\pi\xi_n s]$, are the basis of the modulation of the received signal. The value of g_n for each pixel in the SAR image can be written as:

$$g_n = \sum_{l=1}^{L} \gamma(s_l)\exp[-j\,2\pi\xi_n s_l] + \varepsilon_n \quad n=1,2,...,N \quad l=1,2,...,L \tag{4}$$

where $\gamma(s_l)$ = reflectivity power for the position of s_l

This estimator minimizing the criterion of $\mathrm{E}\{|\boldsymbol{\gamma}(s)^{\mathrm{H}}\mathbf{g}|^2\} = \mathrm{E}\{|\boldsymbol{\gamma}(s)^{\mathrm{H}}\mathbf{g}\mathbf{g}^{\mathrm{H}}\boldsymbol{\gamma}(s)|^2\} = \boldsymbol{\gamma}(s)^{\mathrm{H}}\mathbf{C_g}\boldsymbol{\gamma}(s)$ finds the vector of predictive coefficients $\boldsymbol{\gamma}(s)=[\gamma(s_1),\gamma(s_2),...,\gamma(s_L)]$. The LP technique minimizes the criterion subject to the constraint of unity of the the weight vector for the chosen position in the elevation direction. This restriction can be expressed as:

$$\boldsymbol{\gamma}(s)^{\mathrm{H}}\mathbf{u} = 1 \tag{5}$$

where $\mathbf{u}$ = column vector in the identity matrix $\mathbf{I}_{N\times N}$

The covariance matrix of each pixel in the LP spectral estimation method is calculated using the averaging of neighborhood pixels in both azimuth and range directions:

$$\mathbf{C_g} = \mathrm{E}\{\mathbf{g}\mathbf{g}^{\mathrm{H}}\} \approx \mathbf{C_g} = \frac{1}{K}\sum_{k=1}^{K}\mathbf{g}\mathbf{g}^{\mathrm{H}} \tag{6}$$

where $\mathrm{E}[.]$ = Expectation operator

$(.)^{\mathrm{H}}$ = Hermitian operator

K = total number of adjacent pixels for the averaging

The Lagrange multiplier technique in the LP estimator is employed to find the optimal LP weight vector and the power spectrum by equations (7), (8).

$$\boldsymbol{\gamma}_{\mathrm{opt}}(s) = \frac{\mathbf{C}_g^{-1}\mathbf{u}}{\mathbf{u}^{\mathrm{H}}\mathbf{C}_g^{-1}\mathbf{u}} \tag{7}$$

$$\mathbf{P}_{\mathrm{LP}}(s) = \frac{\mathbf{u}^{\mathrm{H}}\mathbf{C}_g^{-1}\mathbf{u}}{|\mathbf{u}^{\mathrm{H}}\mathbf{C}_g^{-1}\mathbf{A}|^2} \tag{8}$$

2.2.3 Maximum Entropy Estimation Algorithm: The maximum entropy estimator is equivalent to the least-squares fitting of the autoregressive time series model to the input data. The covariance matrix extrapolation as the basis of this technique is carried out to achieve signal entropy maximization. The ME estimator aims to search the autoregressive coefficients such that the expected prediction error of the optimization problem is minimized subject to the $\boldsymbol{\omega}\mathbf{e_1}$ condition, where $\boldsymbol{\omega} = [\omega_1,\omega_2,...,\omega_N]$ and $\mathbf{e_1} = [1,0,...,0]$ are the autoregressive coefficients vector and first column in the identity matrix, respectively. This estimator uses the Lagrange multiplier algorithm to solve the AR coefficients in the optimization problem. The AR coefficients and power spectrum in the ME estimator can be given by equations (9) and (10):

$$\boldsymbol{\omega} = \frac{\mathbf{C_g}^{-1}\mathbf{e_1}}{\mathbf{e_1}^{\mathrm{T}}\mathbf{C_g}^{-1}\mathbf{e_1}} \tag{9}$$

$$\mathrm{P}_{\mathrm{ME}}(s) = \frac{1}{\left|\mathbf{A}^{\mathrm{T}}\mathbf{C}_j\right|^2} \tag{10}$$

where $\mathbf{C}_j$ = j th vector in the inverse covariance matrix

2.2.4 Minimum Norm Estimation Algorithm: This estimator as a subspace algorithm is known in DOA estimation. In this method, SVD is used to decompose the covariance matrix into three component matrices, such as $\mathbf{C_g} = \mathbf{USV}^{\mathrm{T}}$. The noise subspace is excluded from the signal by eigenvectors corresponding to small eigenvalues of the $\mathbf{U}$ so that $\mathbf{U}_{\mathrm{Noise}} = \mathbf{U}(:, q+1:N)$. The number of the largest eigenvalues in the covariance matrix is defined with q. In this method, the finding of the optimal weight vector $\mathbf{d} = [d_1, d_2, ..., d_N]^{\mathrm{T}}$ can be determined as a linear combination of noise eigenvectors. For the assignment problem, the optimal solution can be expressed:

$$\min \mathbf{d}^{\mathrm{H}}\mathbf{d}, \quad \mathbf{U}_{\mathrm{Signal}}{}^{\mathrm{H}}\mathbf{d}=0, \quad \mathbf{d}^{\mathrm{H}}\mathbf{e_1} = 1 \tag{11}$$

In column vector of $\mathbf{e_1}$, the components are all zeros, except one that equals 1. $\mathbf{U}_{\mathrm{Signal}} = [\mathbf{u}_1, \mathbf{u}_2, ..., \mathbf{u}_q]$ in equation (11), is constructed using the eigenvectors corresponding to the largest eigenvalues of the estimated covariance matrix. The first column of the $N\times N$ identity matrix satisfies this necessary condition. In the MN method, the solution to the optimization problem yields the equation's power spectrum:

$$\mathrm{P}_{\mathrm{MN}}(s) = \frac{1}{|\mathbf{A}^{\mathrm{T}}\mathbf{U}_{\mathrm{Noise}}\mathbf{U}_{\mathrm{Noise}}{}^{\mathrm{H}}\mathbf{e_1}|^2} \tag{12}$$

3. STUDY AREA AND DATASET

For the present research, the selected study area is Eskan towers at the intersection of these two main streets, Mirdamad and Vali-e-Asr, in the north of Tehran, Iran. Eskan project comprised three buildings with latitude and longitude of 35°45'50.16"N and 51°24'39.85"E, respectively. Due to

different scatters interfering from these three buildings, the selected building is known as a complicated study area. In this paper, the test building with a height of 72 m covers a subset of the image with pixels. Figure 1 shows the location of the Eskan towers on Google Earth and the corresponding mean amplitude of TerraSAR-X images.
To evaluate the performance of the proposed TomoSAR algorithms based on the nonparametric spectral estimators, we have acquired a stack of 19 stripmap images from a descending orbit over the city of Tehran, Iran. TerraSAR-X took the SAR images between 2012 and 2013, with a 1.2 m range resolution and 3.3 m azimuth resolution. The employed spaceborne satellite provides data from a HH polarization in this paper. The value of the total spatial baseline distribution span for 19 SAR observations is 414 m, resulting in a Rayleigh elevation resolution of about 21 m.

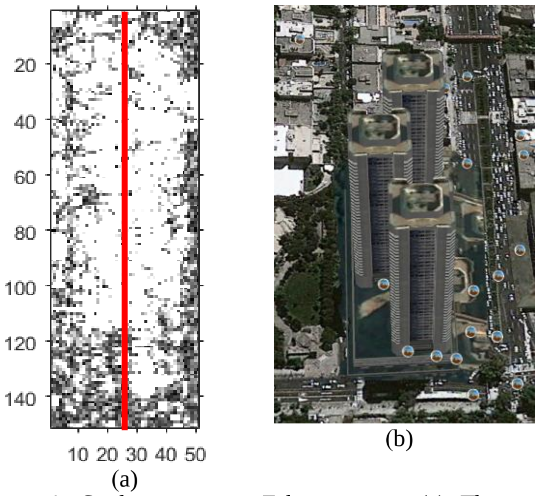

Figure 1. Study area over Eskan towers. (a) The average amplitude of 19 SAR images. (b) The position of the towers.

4. EXPERIMENTS AND RESULTS

This section attempts to analyze the impact of the number of SAR image observations in tomographic reconstruction. Robust detection of scatterers at elevation differences lower than the Rayleigh resolution and estimation of their heights are evaluated in the simulation of TerraSAR-X data stacks. To this aim, several numbers of SAR images are simulated, $N = 19$, $N = 31$, and $N = 65$, with the same total baseline in each scenario.

Figure 2 illustrates the reconstructed reflectivity profiles obtained by six nonparametric spectral estimation techniques, LP, ME, MN, SVD, Capon, and BF. It can be found that increasing the number of SAR acquisitions, ME, MN, SVD, Capon, and BF can resolve the scatterers interfering in the same pixel. The proposed nonparametric LP estimator provides the super-resolution capability and allows the detection of the two scatters located at distances lower than Rayleigh resolution while using a small number of SAR observations. The presented results show that this proposed method is robust to the number of employed images, while other algorithms, such as SVD, ME, Capon, MN, and BF, depend on the number of looks.

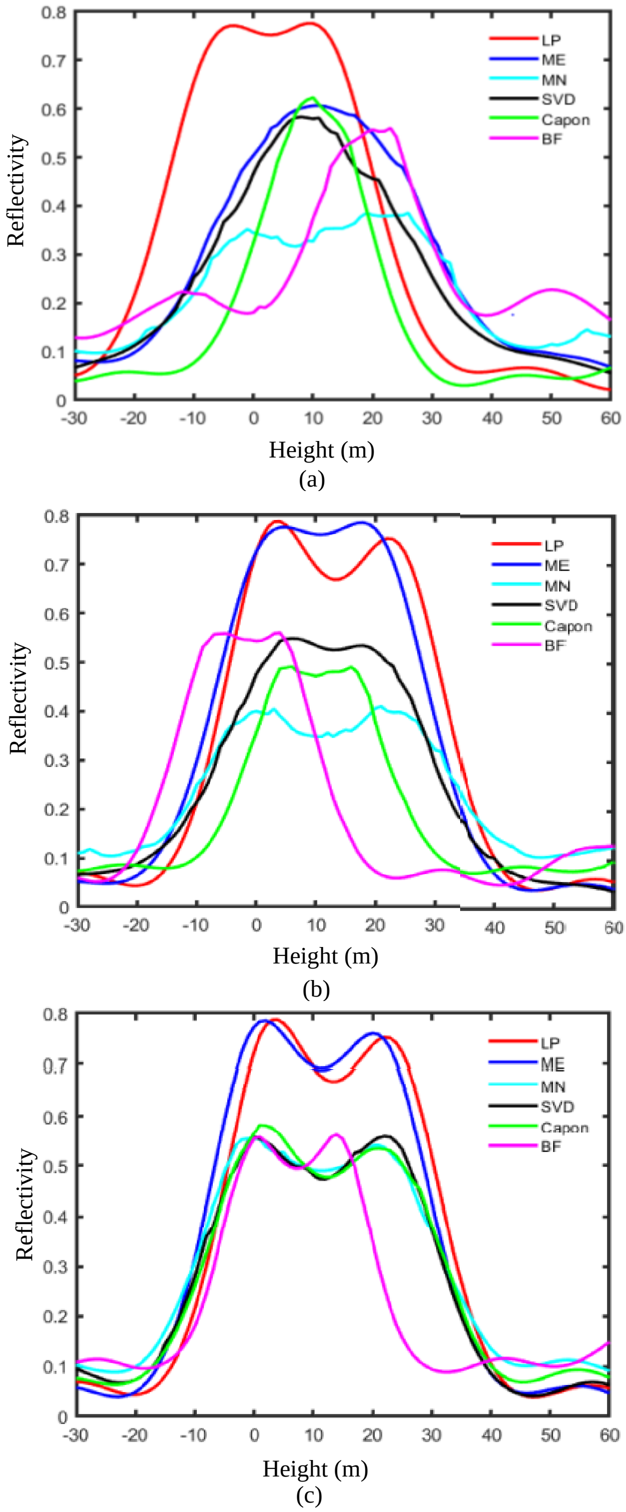

Figure 2. reflectivity profile with the different number of simulated data. (a) 19 observations. (b) 31 observations. (c) 65 observations.

As shown in Figure 1, the side-looking imaging geometry makes interpreting the buildings from urban SAR images highly challenging. The top of Eskan tower appears near range, whereas the response from the bottom of the building study is at the far range. In SAR images, more than one scatterer is mapped onto one pixel due to the interaction between the building facades and the ground. Figure 3 illustrates the results of the tomographic reconstruction using the nonparametric estimators such as the LP, ME, MN, SVD, Capon, and BF along the vertical red marked within the mean amplitude SAR image.

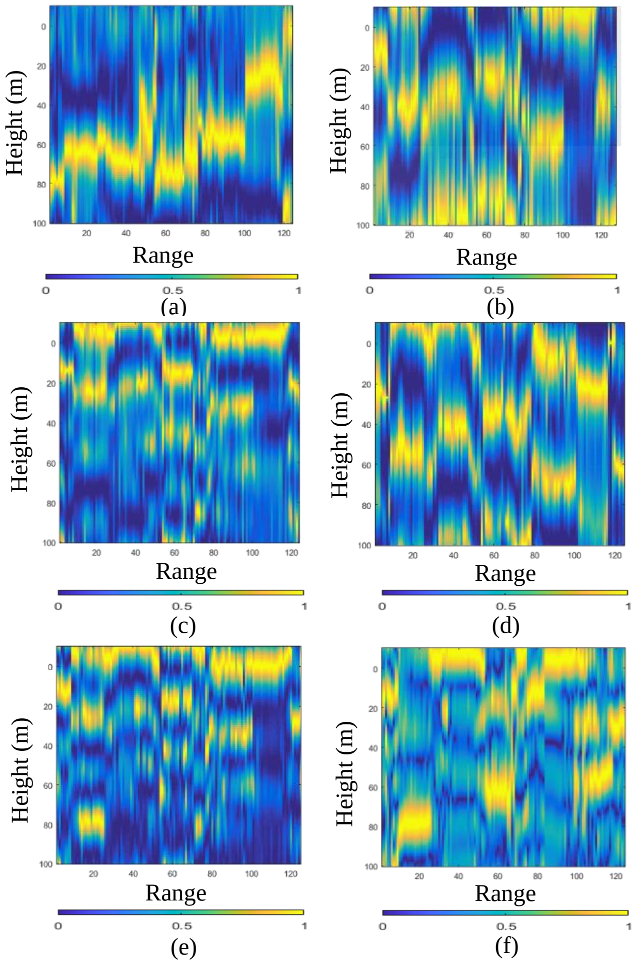

Figure 3. Tomographic reconstruction using nonparametric spectral estimation method. (a) LP. (b) ME. (c) MN. (d) SVD. (e) Capon. (f) BF.

The obtained results indicate the nonparametric LP estimation algorithm's ability to reduce noise levels, reconstruct continuous reflectivity profiles, separate the overlaid scatterers inside an image pixel, and improve the Eskan height estimation. As depicted in this figure, the reconstructed tomographic profiles by SVD, MN, Capon, ME, and BF methods suffer from severe sidelobe interference, the inability to discriminate the contribution of the possible layover scatterers at different heights, the jumping at different heights in the tomograms and the considerable differences between the building height estimation and ground-based measurement of the Eskan case study building. However, the height estimated with the proposed LP estimator from the difference between the top and bottom sections of the Eskan building is 75 m, 3 m height difference with reference data. Table 1 presents the estimated heights using the employed nonparametric spectral estimation methods and their differences with the actual value of the Eskan building height.

Method	LP	ME	MN	SVD	Capon	BF
Estimated Height (m)	75	60	-11	-39	-14	-11
Difference (m)	-3	12	83	111	86	83

Table 1. Estimated building heights and their differences

5. CONCLUSION

In this paper, we presented nonparametric spectral estimation techniques to improve the urban area's building reconstruction and height estimation using a stack of 19 TerraSAR-X stripmap images. To analyze the effectiveness of the proposed TomoSAR techniques, the Eskan building at the intersection of Mirdamad and Vali-e-Asr streets in Tehran, Iran, was selected. In the Eskan project, this building is known as a case study with complex geometry due to the placement of the three buildings with equal height adjacent to each other and the high probability of multiple scattering interference. Compared to the other employed spectral estimation algorithms, such as SVD, MN, Capon, and BF, the obtained results verify the capability of the LP estimator method to resolve different scattering contributions in a SAR image, suppress the sidelobe level and height discontinuity in the tomogram, and improve the accuracy of building height estimation. The estimated height of the test building is near field-based measurement. Also, the results of simulated data indicate the ability of the proposed LP to separate two scatterers below the Rayleigh resolution while using the small number of SAR acquisitions.

ACKNOWLEDGMENTS

The authors thank the Iran National Science Foundation (INSF) for financial support.

REFERENCES

Bamler, R., Hartl, Ph., 1998. Synthetic Aperture Radar Interferometry. *Inverse Problems.* 14(4), R1-R54.

Baselice, F., Budillon, A., Ferraioli, G., Pascazio, V., 2009. Layover Solution in SAR Imaging: A Statistical Approach. *IEEE Geoscience and Remote Sensing Letters.* 6(3), 577-581.

Fornaro, G., Serafino, F., Soldovieri, F., 2003. Three-Dimensional Focusing with Multipass SAR Data. *IEEE Transactions on Geoscience and Remote Sensing.* 41(3), 507-517.

Franceschetti, G., Lanari, R., 1999. *Synthetic Aperture Radar Processing. pace Data from Earth Sciences*. CRC Press, Boca Raton, 60-71.

Gamba, J., 2020. *Radar Signal Processing for Autonomous Driving*. Springer, Japan, 62-86.

Gini, F., Lombardini, F., Montanari, M., 2002. Layover Solution in Multibaseline SAR Interferometry. *IEEE Transactions on Aerospace and Electronic Systems.* 38(4), 1344-1356.

Makhoul, J., 1975. Linear prediction: A tutorial review. *Proceeding of the IEEE*. 63(4), 561-580.

Omati, M., Sahebi, M.R., Aghababaei, H., 2021. Evaluation of Nonparametric SAR Tomography Methods for Urban Building Reconstruction. *IEEE Geoscience and Remote Sensing Letters.* 19, 1-5.

Reigber, A., Moreira, A., 2000. First Demonstration of Airborne SAR Tomography Using Multibaseline L-Band Data. *IEEE Transactions on Geoscience and Remote Sensing.* 38(5), 2142-2152.

Wei, L., Balz, T., Liao, M., Zhang, L., 2014. TerraSAR-X StripMap Data Interpretation of Complex Urban Scenarios with 3D SAR Tomography. *Journal of Sensors.* 2014, 1-8.

Zhu, X.X., Bamler, R., 2010. Tomographic SAR Inversion by L_1-Norm Regularization – The Compressive Sensing Approach. *IEEE Transactions on Geoscience and Remote Sensing.* 48(10), 3839-3846.